(1)

AD-A233 085

RTI

RESEARCH TRIANGLE INSTITUTE

RTI/3629/90-Quarterly

March 1991

SEMICONDUCTOR DIAMOND TECHNOLOGY

Quarterly Report -- Third Quarter
1 July 1990 - 30 September 1990

R. J. Markunas
R. A. Rudder
J. B. Posthill
R. E. Thomas

STRATEGIC DEFENSE INITIATIVE ORGANIZATION
Innovative Science and Technology Office

Office of Naval Research
Program No.
N00014-86-C-0460

POST OFFICE BOX 12194 RESEARCH TRIANGLE PARK, NORTH CAROLINA 27709-2194

REPORT DOCUMENTATION PAGE

Form Approved
OMB No 0704-0188

1. AGENCY USE ONLY *(Leave blank)*	2. REPORT DATE	3. REPORT TYPE AND DATES COVERED
		Quarterly Report, 1 July 1990 - 30 September 90

4. TITLE AND SUBTITLE
Semiconductor Diamond Technology

5. FUNDING NUMBERS
N00014-86-C-0460

6. AUTHOR(S)
R.J. Markunas, R.A. Rudder, J.B. Posthill, R.E. Thomas

7. PERFORMING ORGANIZATION NAME(S) AND ADDRESS(ES)
Research Triangle Institute
P.O. Box 12194
Research Triangle Park, NC 27709

8. PERFORMING ORGANIZATION REPORT NUMBER
~~8350-3629~~

9. SPONSORING/MONITORING AGENCY NAME(S) AND ADDRESS(ES)
Office of Naval Research
800 N. Quincy Street
Arlington, VA 22217-5000

10. SPONSORING/MONITORING AGENCY REPORT NUMBER

11. SUPPLEMENTARY NOTES

12a. DISTRIBUTION/AVAILABILITY STATEMENT
Approved for public release; unlimited distribution

12b. DISTRIBUTION CODE

13. ABSTRACT *(Maximum 200 words)*

This report surveys the progress in a number of research activities pursued this quarter at Research Triangle Institute.

- Gas phase analysis in diamond producing discharges
- Determination of substrate effects on the growth of homoepitaxial diamond
- F_2/CH_4 gas interactions as a function of temperature
- Hydrogen-halogen exchange reactions
- Fabrication and testing of a diamond IGFET, and
- Investigation of LiF as an in-situ dopant for diamond.

These parallel efforts are designed to advance the state-of-the-art in semiconducting diamond technology. These efforts are encompassing development of doping and fabrication techniques for diamond devices while they are also developing novel deposition techniques targetting successful heteroepitaxial growth.

14. SUBJECT TERMS

15. NUMBER OF PAGES
46

16. PRICE CODE

17. SECURITY CLASSIFICATION OF REPORT	18. SECURITY CLASSIFICATION OF THIS PAGE	19. SECURITY CLASSIFICATION OF ABSTRACT	20. LIMITATION OF ABSTRACT
UNCLASSIFIED	UNCLASSIFIED	UNCLASSIFIED	

TABLE OF CONTENTS

LIST OF FIGURES

1.0 INTRODUCTION

This quarterly report contains information on going during the time period from July 1, 1990 to September 31, 1990. It surveys the progress in a number of research activities pursued under the SDIO/IST program. As such it contains information on :

- Gas phase analysis in diamond producing discharges
- Determination of substrate effects on the growth of homoepitaxial diamond
- F_2/CH_4 gas interactions as a function of temperature
- Hydrogen-halogen exchange reactions
- Fabrication and testing of a diamond IGFET
- Investigation of LiF as an in-situ dopant for diamond

Almost all sections in this report have been submitted to the Electrochemical Society Meeting in Washington, May 1991. The work on hydrogen-halogen exchange was presented and published in Fall 1990 MRS Meeting. This spectrum of work is quite diverse. Workers at Research Triangle Institute wish to acknowledge the Raman support provided by R.J. Nemanich and T.P. Humphreys of North Carolina State University, the collaborative support of K. Das and V. Venkatesan, of Kobelco, in fabrication of Schottky contacts for electron beam induced current images of Li doped samples, and the collaborative assistance of David Black at Brookhaven for x-ray topography of diamond substrates.

2.0 GAS PHASE ANALYSIS IN DIAMOND-PRODUCING LOW PRESSURE DISCHARGES

Many workers are studying the importance of acetylene and methyl radicals in the vapor phase growth of diamond. Techniques such as infrared diode laser absorption spectroscopy and multiphoton ionization have been used to examine the gaseous environment of the diamond deposition.[1] In the work reported here, quadrupole mass spectroscopy has been used to monitor acetylene production during diamond deposition in a low pressure rf-plasma chemical vapor deposition environment. We find in a low pressure rf plasma environment that there are two channels for acetylene production. First, CH_4 introduction into the plasma results in a conversion of ~ 60% of the CH_4 into C_2H_2. Second, acetylene is produced via conversion of graphite into C_2H_2. A graphite to C_2H_2 conversion can be distinguished from a graphite to CH_4 to C_2H_2 conversion through independent introduction of CH_4 into the plasma. Furthermore, we find that the diamond deposition rate scales with the rate of acetylene production from graphite.

Polycrystalline diamond depositions have been obtained using a 13.56 MHz rf discharge with 1% CH_4 in H_2 at pressures between 1 and 10 Torr. Details of the reactor and operating conditions have been previously reported[2]. Characterization of the films by Raman scattering shows a distinctive 1332 cm^{-1} diamond line on all films. The environment of the diamond growth was probed by mass spectroscopic analysis of gasses downstream from the plasma region. Samples were positioned near the rf coil on a graphite susceptor. By comparing the C_2H_2 production observed with the

graphite susceptor removed from the discharge tube with the C_2H_2 production when the susceptor was positioned near the rf coil, one can distinguish CH_4 conversion to C_2H_2 from graphite gasification to C_2H_2. (It should be noted that these experiments were performed when the plasma tube was fairly clean of carbon deposits. The graphite susceptor represents the largest source of solid carbon exposed to the plasma).

Figure 2.1 shows the conversion of CH_4 to C_2H_2 as a function of total pressure when the graphite susceptor is not present in the reactor. This figure shows a nearly constant ratio of CH_4 to C_2H_2 across the pressure series. Given that two CH_4 molecules are necessary for C_2H_2 production, we conclude that approximately 60% of the CH_4 is converted into C_2H_2. Figure 2.2 shows the observed C_2H_2 production when the graphite susceptor is inserted 3.0 mm below the rf coil with 1% CH_4 in H_2 discharge. There is a pronounced pressure dependence to the C_2H_2 production. At 3 Torr, there is approximately 4 times more C_2H_2 partial pressure in the reactor with the graphite susceptor present than there was with the graphite susceptor absent. More C_2H_2 is being produced at 3 Torr by graphite gasification than is produced by CH_4 conversion into C_2H_2.

Measurements of the diamond deposition rate as a function of pressure were made from samples grown while mounted on the graphite susceptor. Figure 2.3 shows the deposition rate for a pressure series from 1 to 10 Torr. The deposition rate was determined from cleaved-cross sectional scanning electron micrographs. We find that the deposition rate is a maximum for a pressure of approximately 3 Torr. A comparison with Figure 2.2 shows that acetylene production is correlated with diamond growth

rate and also reaches a maximum at 3 Torr. In order to better understand the graphite gasification to C_2H_2, highly oriented polycrystalline graphite substrates were exposed to the diamond-producing discharges. Micro-Raman scattering has been obtained from regions showing diamond growth on the graphite and from regions showing no growth. The results indicate for the regions between growth, that either a thin layer has formed on the surface or the surface has been disordered.

1. F.G. Celii, P.E. Pehrsson, H.-T. Wang, and J.E. Butler, Appl. Phys. Lett. 52 , 2045 (1988).

2. R.A. Rudder, G. C. Hudson, Y. M. LeGrice, M.J. Mantini, J.B. Posthill, R.J. Nemanich, and R.J. Markunas, Mat. Res. Soc. EA-19 , 89 (1989).

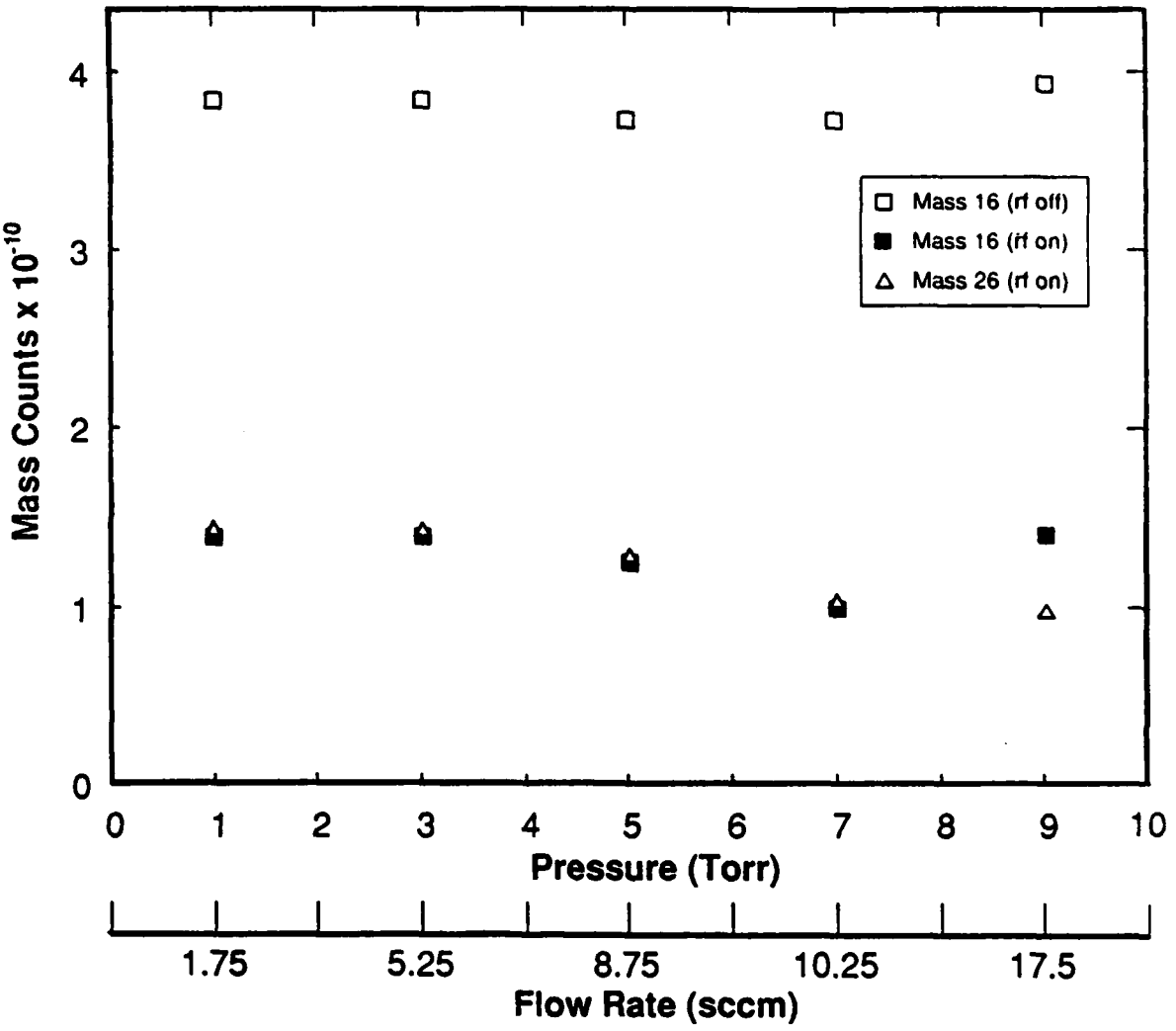

FIGURE 2.1. CH_4 - C_2H_2 conversion as a function of total pressure <u>without</u> the graphite susceptor in position underneath the rf coil.

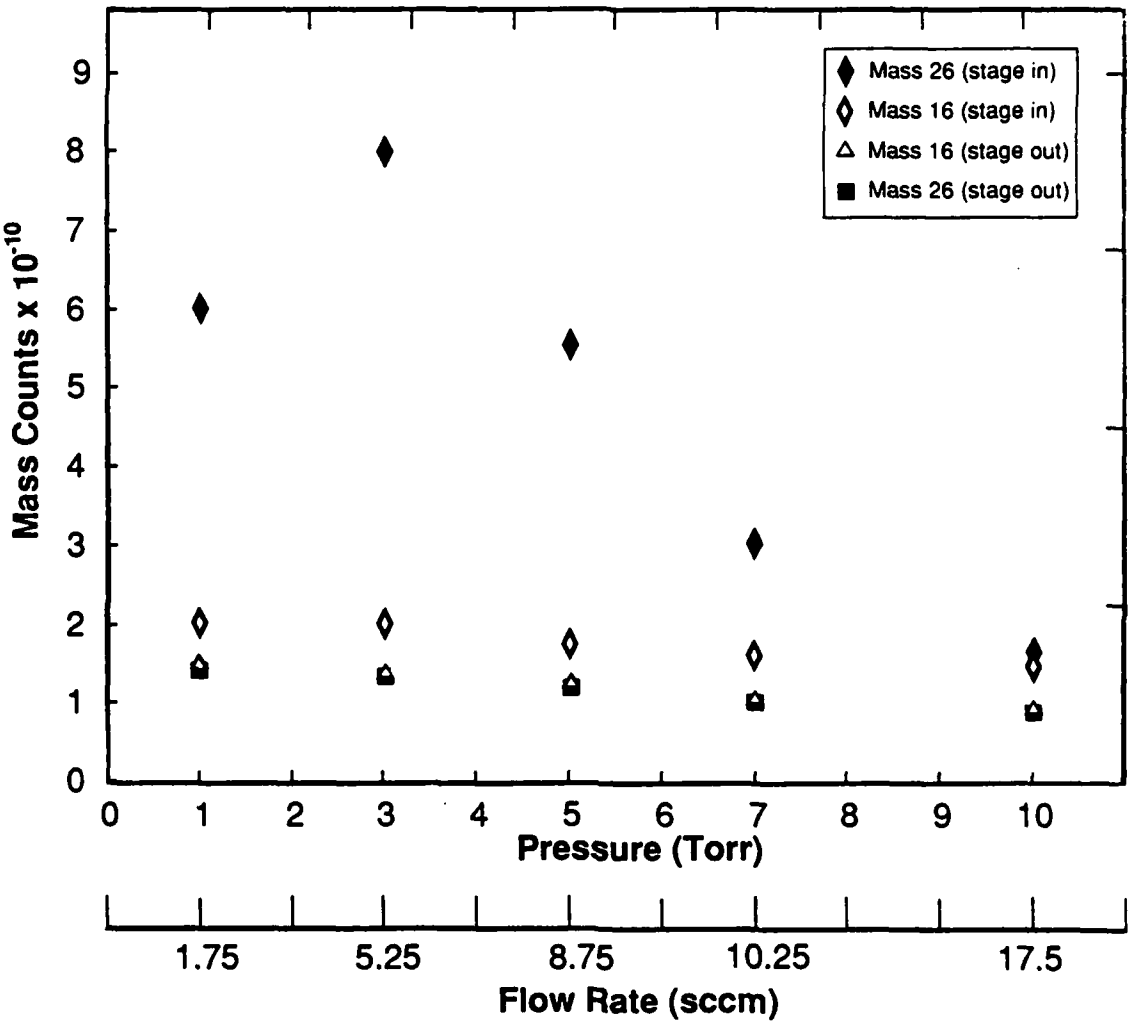

FIGURE 2.2. CH_4 - C_2H_2 conversion as a function of total pressure with the graphite susceptor in position underneath the rf coil.

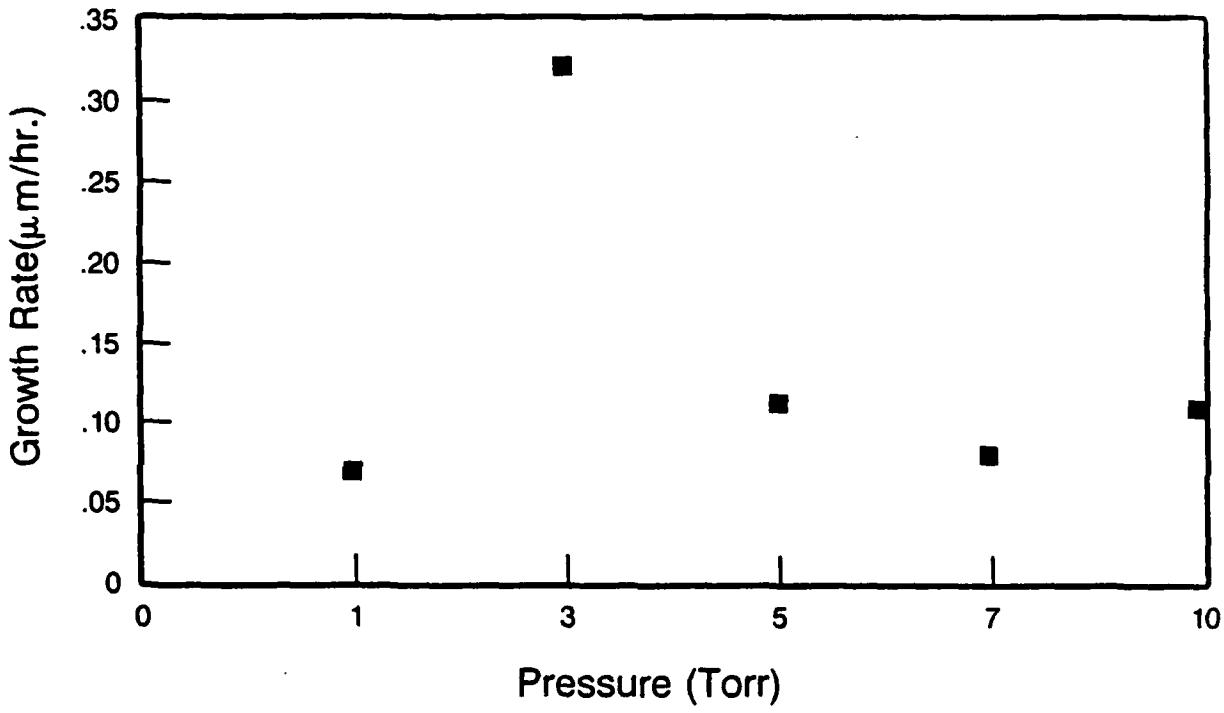

FIGURE 2.3. **Polycrystalline diamond deposition rate as a function of total pressure. Rates determined from cleaved-section SEM analysis.**

3.0 DETERMINATION OF SUBSTRATE EFFECTS ON THE GROWTH OF HOMOEPITAXIAL DIAMOND

The thermal and electrical properties of diamond make it an excellent candidate for electronic applications. A number of significant problems must be overcome before the potential of diamond can be realized. While suitable heteroepitaxial substrates have not been developed yet, the fabrication of diamond transistors on natural diamond substrates allows testing and evaluation of diamond electronics. One problem arising in the fabrication of diamond devices on diamond is the quality of the natural diamond substrates. Recent studies indicate that x-ray topography is a potentially valuable technique for characterizing structural defects in diamond single crystal substrates[1]. Selection of high quality diamond substrates is imperative to the growth of high mobility homoepitaxial layers. In order to achieve the highest mobilities, growth techniques may have to developed which deposit epitaxial layers without replicating the crystalline defects commonly found in diamond single crystals.

Natural diamond substrates have been evaluated using x-ray topography and scanning electron microscopy (SEM) to qualify the substrate quality and the surface polish before homoepitaxial diamond growth. SEM and Raman spectroscopy have been used to characterize the epitaxial films after growth. X-ray topography has revealed differences in the bulk structure of type Ia and type IIa diamonds. Although the type Ia diamonds appear to show square facets in projection. there appear to be fewer defects in type Ia crystals. This is qualitatively consistent with the observations that type Ia diamond crystals tend to exhibit superior axial ion channeling

characteristics than type IIa crystals.[2] While these results appear to indicate a trend, it must be borne in mind that variations between different natural diamond crystals may not permit these results to be generally applicable to all diamond substrates of a given type. Features are seen on the surface which might inhibit high quality epitaxial growth. Figure 3.1(a) shows a SEM micrograph of an as-received natural Type IIa diamond (100) surface. Although the surface topographies do vary from substrate to substrate, Figure 3.1 is representative - particularly with regard to the fine, unidirectional scratches that are seen.

The system used for the growth of homoepitaxial diamond consists of a 13.56 MHz inductively-coupled plasma-enhanced chemical vapor deposition (PECVD) system. A gas mixture of *98.8% H_2, 0.6% CO and 0.6% CH_4 flowed through a 62.5 mm quartz* tube at a rate of 30 sccm at 5.0 Torr. The sample is positioned near the rf coil on a graphite susceptor and is held at $\sim$ 800 °C during growth. Figure 3.1(b) shows the change in surface morphology after 1 μm of diamond deposition on a diamond substrate. Before deposition the surface shows pits and polishing scratches present. After deposition, the surface finish is greatly improved as little surface topography is visible.

The effect of surface planarization during homoepitaxial growth can also be illustrated using selective homoepitaxial deposition. Epitaxial lateral overgrowth has been demonstrated using a low pressure rf-plasma assisted chemical vapor deposition technique[3]. A 200 nm thick Si film, deposited on the diamond surface, has been patterned to define "seed" areas for homoepitaxial growth. The overgrowth was revealed by chemically etching the Si from the diamond. Figure 3.2 shows SEM of a cleaved cross-

section showing diamond epitaxial lateral overgrowth. The sample has been sputter-coated with $\sim$ 100 A of Pt to prevent charging. Growth of homoepitaxial diamond was observed to be isotropic - extending over the Si mask by 0.45 μm and above the mask by 0.50 μm. Comparing the surface of the epitaxial layer to the surface of the substrate, the initial substrate topography has been planarized by this diamond homoepitaxial deposition process.

Micro-Raman spectroscopy was employed to assess the crystalline quality of homoepitaxial diamond films. Micro-Raman spectrum showed a 1332 cm^{-1} diamond LO phonon line with a FWHM of 2.1 cm^{-1}. This spectrum was obtained by focusing the incident laser beam (Ar^{+}, 514.5 nm) of $\sim$ 5μm spot size onto the surface of the diamond homoepitaxial film. By changing the depth of focus into the type IIa substrate, the FWHM increased to 2.4 cm^{-1}. Although this technique cannot completely isolate the Raman signals from the epi and the substrate, it shows qualitatively that the homoepitaxial film is of greater perfection than the substrate.

1. Andrew R. Lang, "Cathodoluminescence and x-ray topography of HPHT diamonds", ICDNST-2, Washington, DC, September 23-27, 1990.

2. G.S Sandu, N.R. Parikh, and M.L. Swanson, private communication of unpublished results, University of North Carolina, Chapel Hill, 1989.

3. R.A. Rudder, J.B. Posthill, G.C. Hudson, D.P. Malta, R.E. Thomas, R.J. Markunas, T.P. Humphreys, and R.J. Nemanich, "Selected-area homoepitaxial growth and overgrowth of homoepitaxial diamond on Si patterned diamond substrates", ICDNST-2, Washington, DC, September 23-27, 1990.

Low Pressure rf Plasma Technology Improves Diamond Surface Topography During Diamond Deposition

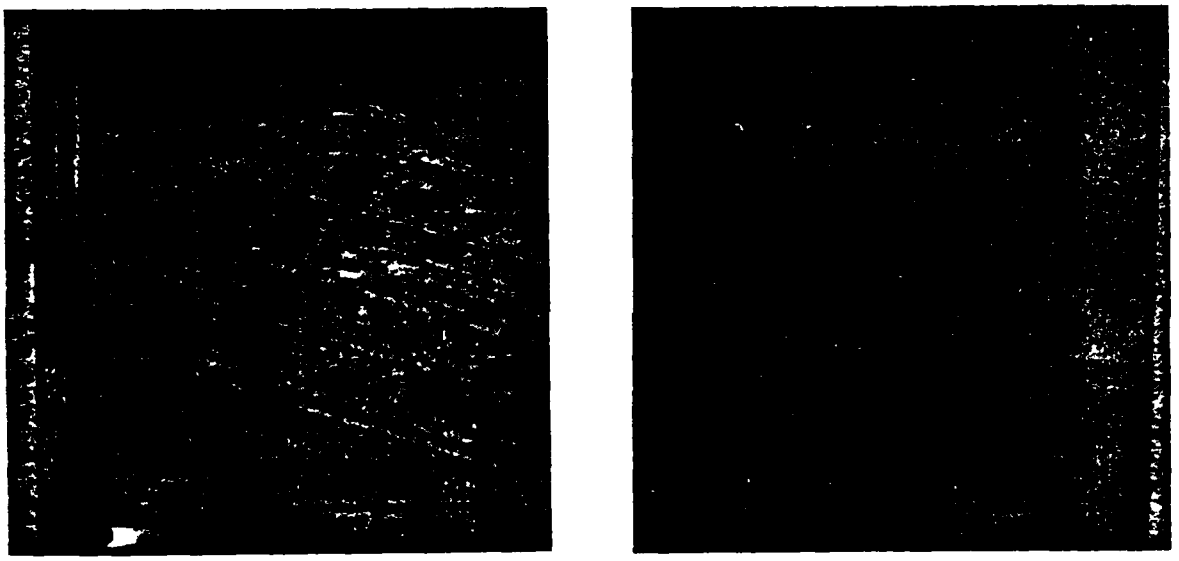

Before Growth **After Growth**

FIGURE 3.1. Representative SEM of a substrate before and after diamond homoepitaxial growth.

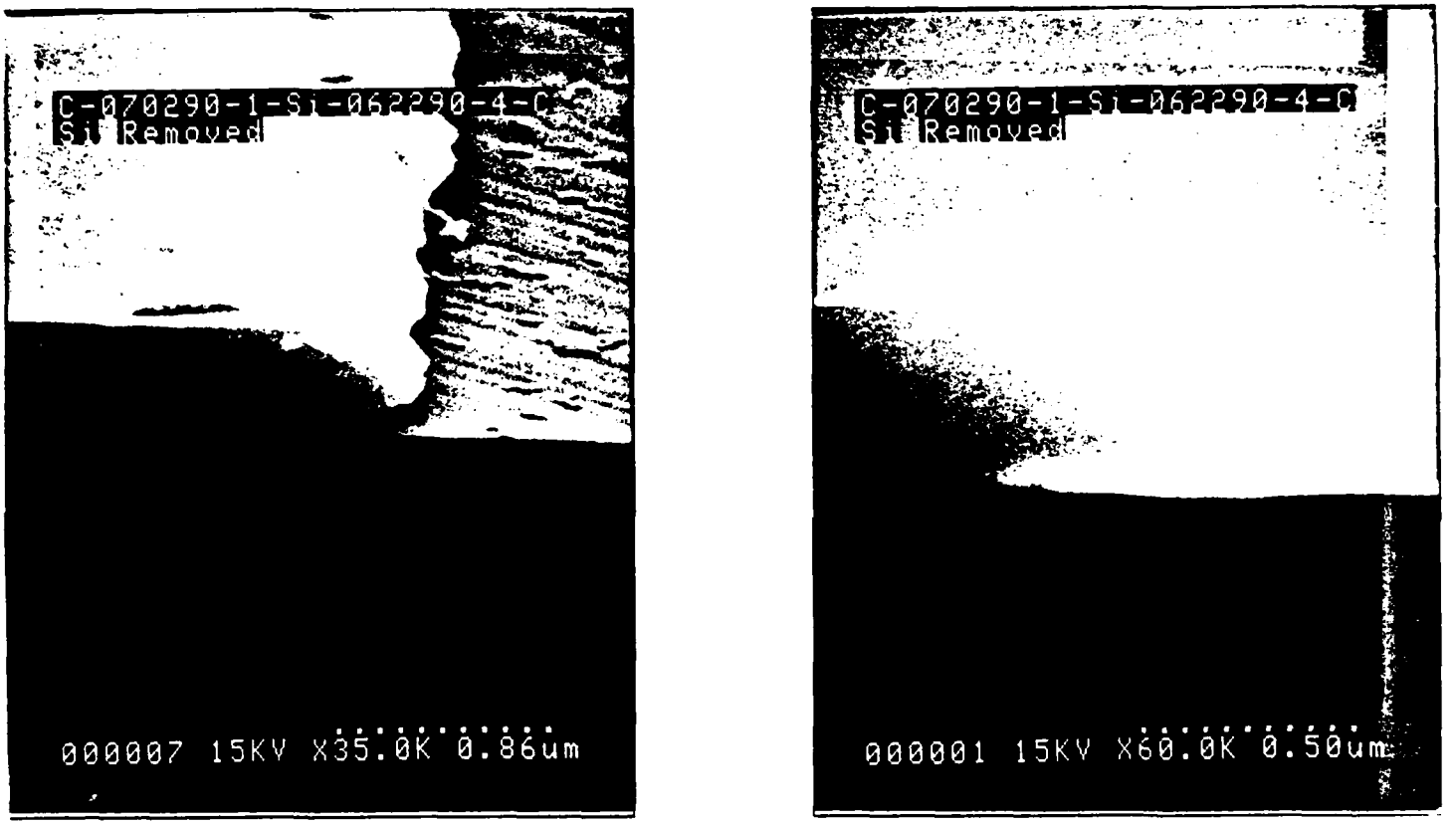

[Has been sputter-coated with ~100Å of Pt to prevent charging]

FIGURE 3.2. SEM of cleaved cross-section showing epitaxial lateral overgrowth of diamond over a Si mask (removed).

4.0 $F_2 - CH_4$ GAS INTERACTIONS ACROSS A HEATED GRAPHITE ELEMENT

Recent work by Patterson, et al.[1] and previous work by Rudder et al.[2] have shown that diamond deposition from a fluorine-based environment is possible. Patterson exploited the use of mixed fluorine-hydrogen chemistries (i.e., F_2 and CH_4) to form solid carbon through a proposed reaction of:

$$CH_4 + 2F_2 \rightarrow C_{(s)} + 4HF \quad (1)$$

The free energy of the reaction would be more exothermic than a corresponding hydrogen-based reaction involving CH_4 and H_2. The hot zone of the Patterson-type reactor operated between 700 and 950 °C, and diamond growth occurred only in regions of the reactor where the temperature was between 250 and 750 °C.

To gain insight into the fluorine-based process, we have utilized quadrupole mass spectroscopy of F_2/CH_4 to analyze gas interactions as a function of temperature. The work is performed in an UHV compatible chamber that is evacuated by a corrosive series, 1000 l/s turbomolecular pump. Gases are admitted into the chamber using mass flow controllers. The pressure in the chamber is maintained at 0.500 Torr for $F_2 - CH_4$ gas work described here. A graphite strip heated is enclosed in the chamber as well as a sample heater stage whereby growth attempts independent of the graphite strip heater can be assessed. The graphite heater is machined from a dense, fine-grain graphite and is not highly oriented pyrolytic graphite. A mass quadrupole operating at low emission (0.25 mA) is used to sample the gases exiting the reactor. Changes in the

gas composition as a function of substrate temperature or the graphite heater temperature are monitored.

To study the interaction of F atoms with both solid carbon such as graphite and with gaseous carbon such as CH_4, a graphite strip heater was installed in the chamber. By adjusting the current through the graphite element, the reactions of F_2 and/or F with the densified graphite can be studied as a function of temperature. One advantage in using a graphite heater to study the F_2/CH_4 gas interactions is that reactions of fluorine with graphite have been previously studied[1] so there exists comparative information. A second advantage to the graphite heater is that it avoids questions of metal catalysis reactions. Figure 4.1 shows the observed CF_3 mass counts in the reactor as a function of temperature. The CF_4 production is observed to decrease for temperatures in excess of 950 ° C. The temperature dependence is convoluted by the fact that there is a substantial temperature variation± 100 ° C across the graphite heater element. Upon introduction of CH_4 into the hot fluorine, the CF_4 production decreases. Fluorine interactions with the CH_4 is the gas phase will deplete the gas phase of fluorine, resulting in a lower incident flux of F atoms to the graphite surface. and a lower production rate of CF_4. This is the first evidence observed for $F_2 - CH_4$ gas interactions. Besides the reduction in CF_4 production, the introduction of CH_4 into the hot fluorine produces HF and C_2F_2H production. Figure 4.2 shows the production of those molecules as a function of the graphite temperature. The temperature dependence for the HF production is more pronounced than the temperature dependence for the C_2F_2H production. Both exhibit a maximum in production around 900 ° C.

This work suggests that the proposed reaction of Patterson, et al. for solid carbon production via equation (1) is basically correct. Our observations of (1) thermal atomic fluorine production, (2) gasification of graphite into CF_4, and the formation of HF and C_2F_2H by-products, suggests that the reaction in equation (1) should be extended.

$$2F_2 \rightarrow^{700\,^{\circ}C} 4F + CH_4 \rightarrow C_{solid} + 4HF$$
$$4F_2 \rightarrow^{700\,^{\circ}C} 8F + 2CH_4 \rightarrow C_2H_2F_2 + 6HF$$
$$2F_2 + C_{graphite} \rightarrow^{500\,^{\circ}C-700\,^{\circ}C} CF_4$$

1. Donald E. Paterson, Benjamin J. Bai, C. Judith Chu, Robert H. Hauge, and John L. Margrave, "Halogen-Assisted Chemical Vapor Deposition", presented at 2nd International Conference on the New Diamond Science and Technology, Washington, DC(USA), September 23-27, 1990.

2. R.A. Rudder, J.B. Posthill, R.J. Markunas, Electronics Lett. 25, 1220 (1989).

3. D.E. Rosner and J. Strakey, J. Phys. Chem. 77, 690 (1973).

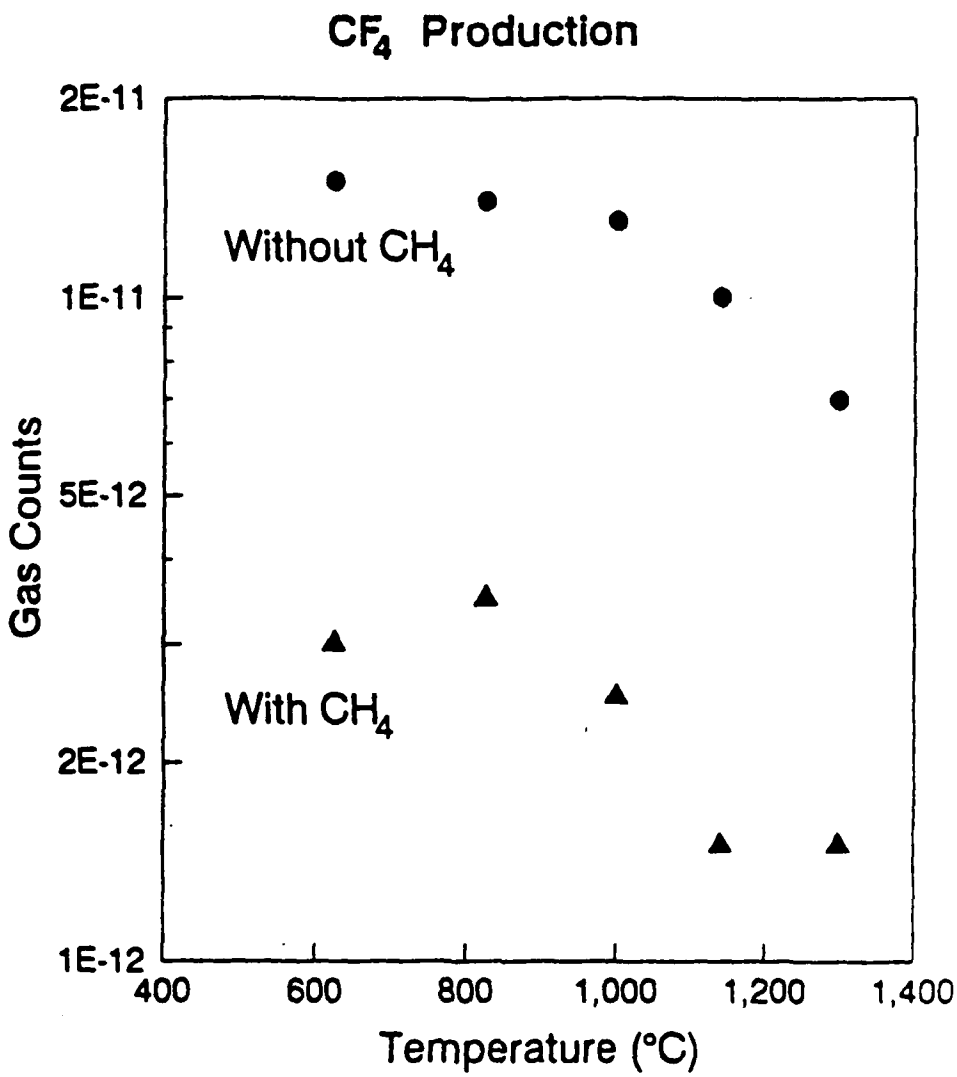

FIGURE 4.1. Interaction of fluorine with a graphite surface as a function of temperature. CF_4 production (as monitored by a CF_3 mass count) was observed prior to CF_4 introduction.

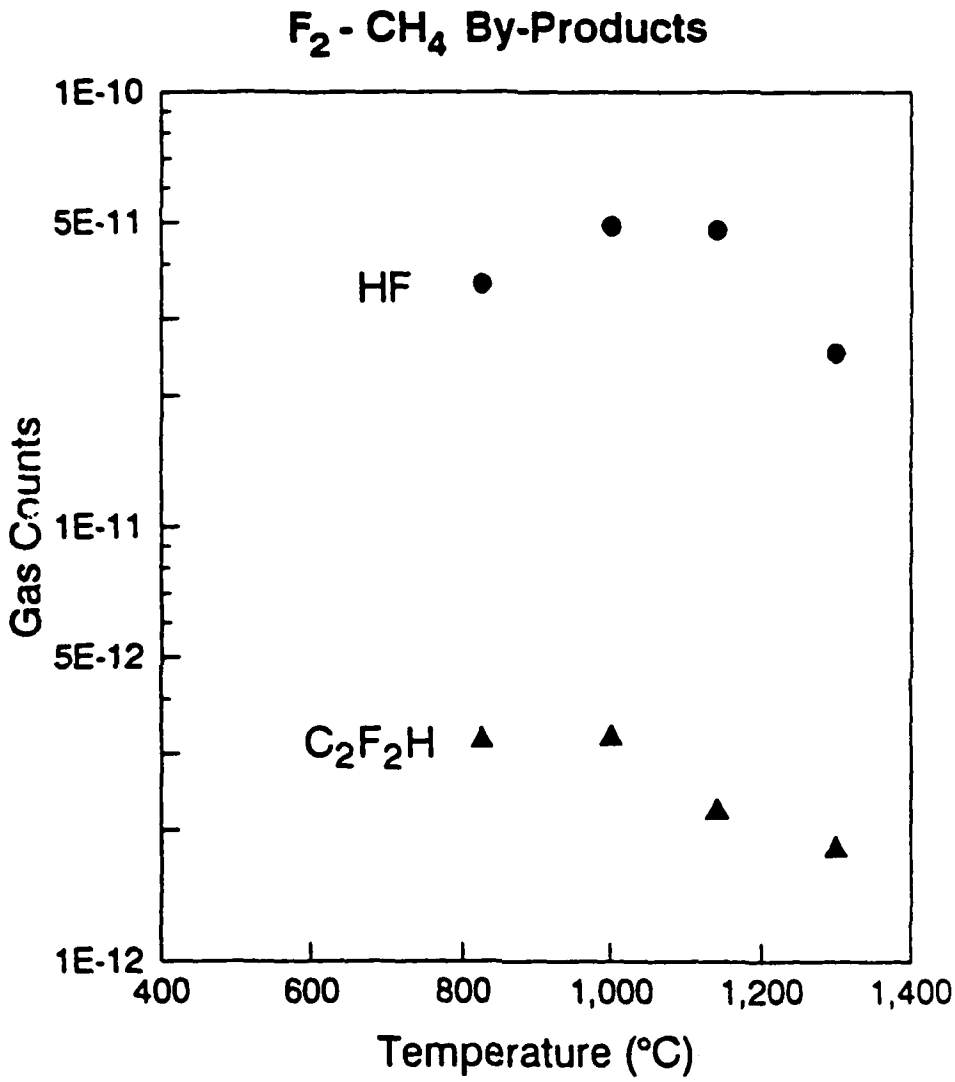

FIGURE 4.2. Production of HF and $C_2F_2H_x$ upon interaction of F_2 and CH_4 with heater graphite.

5.0 HYDROGEN--HALOGEN EXCHANGE REACTIONS

Using thermal mass desorption and LEED we have studied interactions of H, Cl_2, and F_2 with a silicon (100) surface, and exchange reactions of the gases with adsorbates on the silicon (100) surface. Thermal desorption spectra were measured for surfaces dosed with H, Cl_2, and F_2 singly and then for surfaces dosed first with a halogen and then atomic hydrogen. Finally, the reverse sequence was studied, with atomic hydrogen dosing and then the halogen exposure. Results indicate that the molecular halogens Cl_2 and F_2 are not effective at removing H from a Si (100) surface. However, for the reverse reaction, atomic hydrogen appears quite effective at removing the halogens.

5.1 Introduction to Hydrogen-Halogen Exchange Reactions

We are studying hydrogen--halogen interactions on silicon surfaces as part of an overall effort to develop atomic layer epitaxy (ALE) growth cycles for group IV epitaxial thin films. An ALE sequence designed to grow column IV materials is expected to be quite different than methods currently used for II-VI and III-V materials in that one cannot rely on alternating chemistries associated with the semiconductor constituents. A strategy based on changing the terminating surface species holds promise as a substitute. Since the extraction process is expected to be part of a growth cycle at an elevated temperature, studies were also made of the hydrogen/chlorine exchange efficiency as a function of substrate temperature during atomic hydrogen dosing.

5.2 Experimental Procedures

All dosing and desorption work was done in a stainless steel UHV chamber equipped with an Extrel C-50 quadrupole mass spectrometer, a Princeton Research Incorporated LEED apparatus, and an Ircon 15C10 infrared pyrometer with a temperature range of 200 ° C-800 ° C. Base pressure in the main chamber was typically $5x10^{-10}$ Torr. Silicon samples used in the present work were cleaved from 3" (100), n-type, 0.005 ohm-cm, wafers. Normally it is difficult to accurately measure the temperature of silicon via a pyrometer with a fixed emissivity. However with heavily doped silicon the emissivity is much less sensitive to temperature.[1] We estimate emissivity variations of $<.05\%$ over the temperature range of 200 ° C-800 ° C. This corresponds to an uncertainty in the temperature of approximately 10 ° C. To further reduce sample to sample variations in temperature measurement the wafers were factory polished on both sides. Emissivity was set by wire bonding a Pt/Pt-10%Rh thermocouple to a silicon wafer and heating to 550 ° C. The emissivity was then adjusted on the pyrometer to match the thermocouple temperature. Samples were cleaned prior to loading in the chamber by dipping in HF for 2 minutes, and then rinsing in DI water for 5 minutes. The chamber was then evacuated and baked for 2-3 days. Further cleaning of the sample was accomplished in-situ by thermal annealing. The sample was rapidly annealed at successively higher temperatures, taking care to keep the pressure as low as possible--typically $<2x10^{-8}$ Torr. Sharp 1x2:2x1 LEED patterns were obtained using this procedure.

A W filament at approximately 2000 ° C was used for the production of atomic hydrogen. The filament was located 2-3 cm from the silicon surface. Gas flow was controlled with a leak valve and gas was introduced into the chamber through a 0.25" s.s. tube located 3 cm behind the W filament. Dose rate was set by measuring the chamber pressure, and dosing for a predetermined time. For all gases except atomic hydrogen, all filaments are turned off during dosing. After dosing the sample was moved in front of the quadrupole for thermal desorption. Dosing gases used included a 99.99% chlorine source, 99.999% hydrogen, and 2.0% fluorine in helium. All thermal desorption spectra were taken at a heating rate of 5 ° C/sec.

Halogen coverages were not measured directly. Instead, the samples were dosed for a fixed period of time with a series of increasing pressures. After each halogen dose a thermal desorption spectrum was taken and the intensity of the SiCl or SiF_2 peak noted. As the pressure was increased in the desorption series a saturation in the intensity of the desorbed halo-silanes was seen. This saturation occurred at a total dose of 120 x 10^{-6} Torr-seconds for chlorine and at a total dose of 90 x 10^{-6} Torr-seconds for the 2% F_2/He gas mixture.

5.3 Results

Hydrogen/Chlorine Exchange

Three different cases for hydrogen/chlorine exchange were studied: the removal of adsorbed chlorine by dosing with atomic hydrogen, the removal of adsorbed chlorine by dosing with molecular hydrogen, and the removal of adsorbed hydrogen by dosing

with molecular chlorine. Of the combinations studied, it was found that an exchange occurred only when chlorine was adsorbed first and then atomic hydrogen was admitted. Molecular chlorine would not remove adsorbed hydrogen from the silicon surface, and molecular hydrogen would not remove chlorine adsorbed on the surface.

Figures 5.1 and 5.2 show the effects of atomic hydrogen dosing on the thermal desorption spectra of a chlorine dosed sample. Samples held at 25 ° C were first dosed with molecular chlorine and then with atomic hydrogen at varying pressures. The figures track desorbing H_2, and SiCl, as a function of total hydrogen dose. In the hydrogen desorption spectra, Figure 5.1, characteristic peaks appear at 425 ° C and 540 ° C after dosing with atomic hydrogen. These peaks are commonly referred to in the literature as the β_2 and the β_1 peaks respectively.[2] LEED measurements after the hydrogen dosing and prior to desorption confirm the transformation from a 2x1 structure to a 1x1 structure. Figure 5.2 follows the SiCl desorption peak as a function of total dose of atomic hydrogen. We observe that as the total hydrogen dose increases the amount of SiCl subsequently desorbed decreases.

A final series of experiments was performed on the hydrogen/chlorine system to study the effects of substrate temperature on the exchange process. The samples were dosed at 25 ° C with chlorine, then raised in temperature to the desired point, next dosed with atomic hydrogen, cooled to 25 ° C, and finally thermal desorption spectra were taken. In order to be able to follow the effect of the substrate temperature on the chlorine removal the hydrogen dosing pressure, and time were chosen so as to only partially remove the chlorine from the surface.

Figure 5.3 shows a plot of normalized peak counts for SiCl desorption. Data from two groups of samples are shown: samples that were dosed with chlorine and then dosed with atomic hydrogen at an elevated temperature, and for samples dosed with chlorine and annealed at an elevated temperature without hydrogen dosing. For the samples not receiving hydrogen dosing we see little evidence of SiCl desorption until the 600 ° C anneal indicating that the SiCl is relatively stable below the desorption temperature. In contrast, hydrogen extracts an increasing amount of chlorine as the temperature is increased. In general we find that annealing at a given temperature during hydrogen dosing removes peaks in the spectra that had a desorption temperature lower than the annealing temperature. For example, after annealing at 200 ° C the β_2 hydrogen peak remains. However, annealing at 400 ° C removes the β_2 peak. A similar effect was observed for HCl and SiCl desorption peaks.

Hydrogen/fluorine exchange

The results for fluorine are quite similar to what was seen for the chlorine work. The major difference is that SiF_x species desorb at a lower temperature than $SiCl_x$ species. Masses monitored for these experiments were 2, 19, 66, 85, and 86. which corresponds to H_2, F, SiF_2, SiF_3, and SiF_3H, respectively. As in the case of chlorine, LEED indicates that the surface remains in a 2x1 configuration after dosing with F_2. The next series of experiments studied exchange reactions between hydrogen and fluorine. Figures 5.4 and 5.5 show a series of thermal desorption spectra where the sample, held at 25 ° C, was first saturated with molecular fluorine, and then dosed with atomic hydrogen at a series of increasing total doses. We see a steady decline in the

SiF_2 counts as the total hydrogen dose is increased.

Two additional experiments were performed. In the first, samples were dosed with atomic hydrogen to saturation and then exposed to F_2 at 25 ° C. No evidence of SiF_x desorption was seen after this dosing. In the second experiment, samples were dosed with molecular fluorine and then dosed with molecular hydrogen. Again no evidence of exchange was seen.

5.4 Discussion

Hydrogen-chlorine exchange

Thermal desorption temperatures and products for chlorine on silicon reported here are similar to results obtained in earlier studies by Jackman et.al.[3] In their work, two desorption peaks for chlorine on silicon were found: one at 175 ° C, termed the α peak, and another peak at 625 ° C termed the β peak. Jackman et.al. concluded that the low temperature phase is a corrosive phase consisting of $SiCl_4$ which forms after saturation of the β phase. The work reported here was done for the most part in a regime where the β phase was saturated with approximately 1 monolayer of chlorine on the surface. The major difference is that we do not see the growth of the low temperature α phase in the SiCl desorption curves.

For the exchange reactions we find that at room temperature atomic hydrogen will remove chlorine from the silicon surface, while molecular hydrogen will not. In the reverse reaction molecular chlorine will not remove hydrogen from a silicon surface.

Since the HCl bond is 103 KCal/mole and the SiCl bond is 96 Kcal/mole, simple energetics favors the extraction by atomic hydrogen of chlorine adsorbed on silicon. Without adding energy to split the H_2 molecule the energetics do not favor the extraction of chlorine with molecular hydrogen.

For the reaction of molecular chlorine with a hydrogen terminated surface the reaction is actually favored for 2 sequences:

$SiH_2 + Cl_2 \rightarrow SiCl_2 + H_2$ +86 Kcal/mole

$SiH_2 + 2Cl_2 \rightarrow SiCl_2 + 2HCl$ +130 Kcal/mole.

At room temperature there is apparently insufficient energy to overcome kinetic barriers to this reaction.

Since atomic hydrogen is known to etch silicon the possibility exists where the Cl has weakened the Si back bonds sufficiently for the H to extract the chlorine via a $SiCl_xH_y$ species. Work by Cheung and Coburn indicates that the etching of silicon by H terminates once the surface is chlorine terminated.[4] This result supports the conclusion that chlorine extraction by silicon is not accomplished via the formation of $SiCl_xH_y$ species. Further work remains to determine if the product formed during the reaction is HCl.

Note that on energetic grounds atomic chlorine is expected to extract hydrogen from the silicon surface since both HCl (103 Kcal/mole) and Si-Cl (96 Kcal/mole) are favored over the Si-H bond (76 Kcal/mole). It is also likely that once the hydrogen was removed the chlorine would continue to etch the silicon,[4] and the reaction would not

be self-terminating.

Hydrogen/Fluorine exchange

The results for fluorine desorption from silicon described in the present work are quite similar to results obtained by Engstrom et.al.[5] They find that both SiF_2 and SiF_4 desorb from silicon (100) after dosing with molecular fluorine. At monolayer coverages the desorption maxima occur at approximately 525 ° C. It appears that there is little if any shift induced in the desorption temperature of the SiF_2 by the presence of hydrogen on the surface. However, as is the case with chlorine, dosing of a fluorinated silicon surface with atomic hydrogen leads to a reduction in the amount of SiF_x species that are subsequently desorbed.

The bond energies involved however do not favor the exchange as was the case with chlorine and silicon. The HF bond is 136 Kcals/mole and the SiF bond is 143 Kcals/mole so a simple exchange is not expected. Furthermore, the energetics for the exchange of molecular fluorine with adsorbed hydrogen are very large,

$SiH_2 + F_2 \rightarrow SiF_2 + H_2 + 200$ Kcals/mole

$SiH_2 + 2F_2 \rightarrow SiF_2 + 2HF + 330$ Kcals/mole.

Although the bond energies indicate that the reaction is very favorable, in fact more so than for molecular chlorine to extract hydrogen, the kinetic barriers to the reaction are apparently still too large to overcome at 25 ° C. Finally, while the desorption mechanisms for chlorine and fluorine appear to be similar, there is no data available at present

to support the conclusion that fluorine is extracted by hydrogen, via the formation of HF. Atomic fluorine extraction of hydrogen was not studied here, but again one expects the reaction to proceed, perhaps with great vigor.

5.5 Conclusions

Atomic hydrogen will remove both chlorine and fluorine from a silicon (100) surface. Molecular hydrogen in contrast is ineffective at displacing these halogens. Evidence suggests, at least in the case of chlorine, that removal occurs via the formation of HCl rather than a volatile $SiCl_xH_y$ species. Furthermore, the hydrogen/chlorine removal is found to be effective up to the desorption temperature of the $SiCl_x$ species. In spite of the favorable energetics, there was no evidence that either molecular chlorine or molecular fluorine would remove hydrogen from the silicon surface at 25 ° C. Higher temperature experiments are expected to move interaction between the surface hydrogen and the gaseous halogen. This work will be limited to temperatures below 400 ° C. Above 400 ° C, the surface hydrogen would desorb.

1. T. Sato, Jap. Jnl. Appl. Phys. 6, 339 (1967).

2. S.M. Gates, R.R. Kunz, and C.M. Greenlief, Surf. Sci. 207 364 (1989).

3. R.B. Jackman, H. Ebert, and J.S. Foord, Surf. Sci. 176, 183 (1986).

4. M.-C. Chuang, and J.W. Coburn, Jnl. Vac. Sci. Tech. A 8, 1969 (1990).

5. J.R. Engstrom, M.M. Nelson, and T. Engel, Surf. Sci. 215 437 (1989).

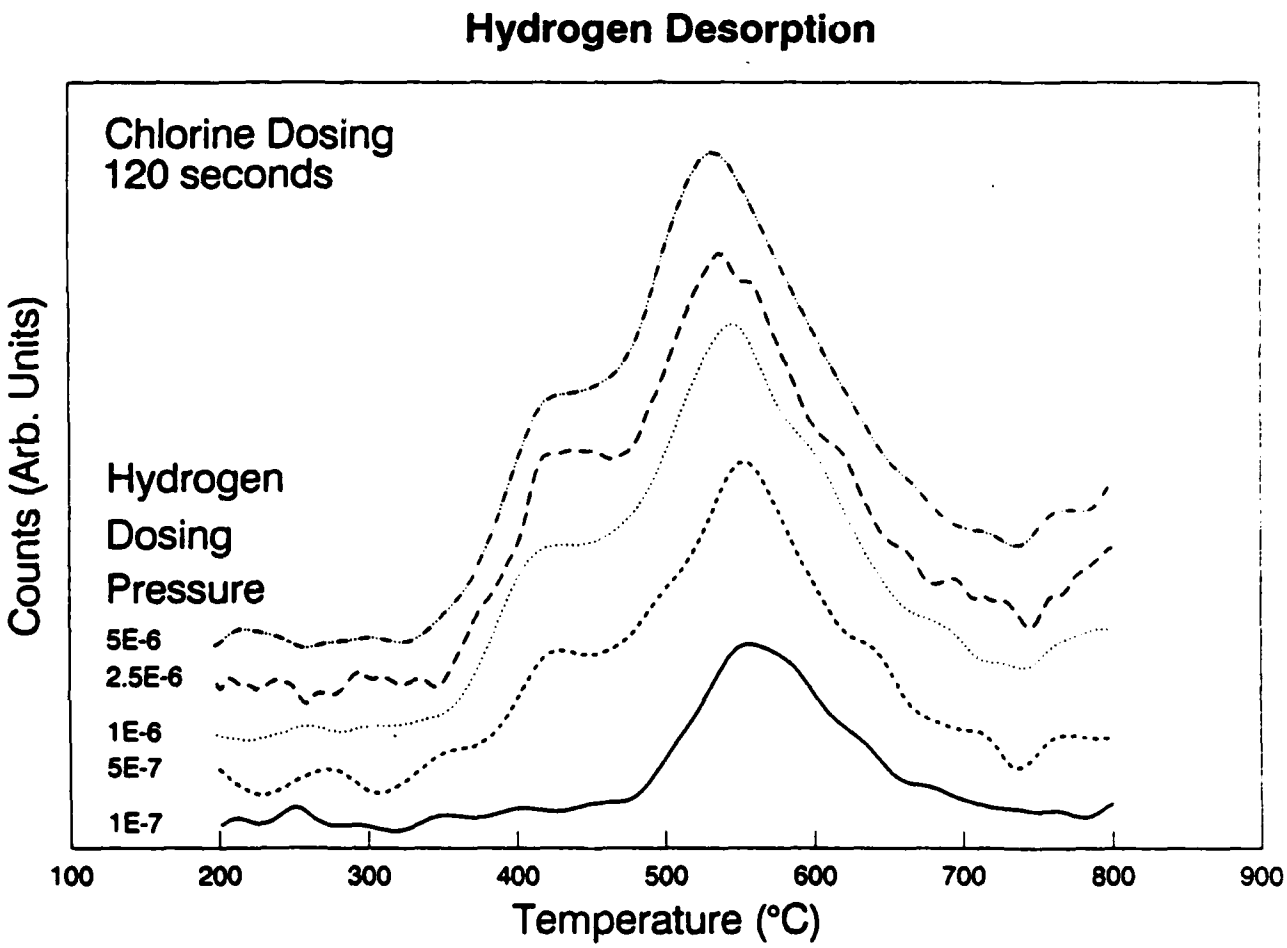

FIGURE 5.1. This figure shows hydrogen desorption from a sample that has been dosed first with molecular chlorine and then with atomic hydrogen at the pressures indicated, (Torr).

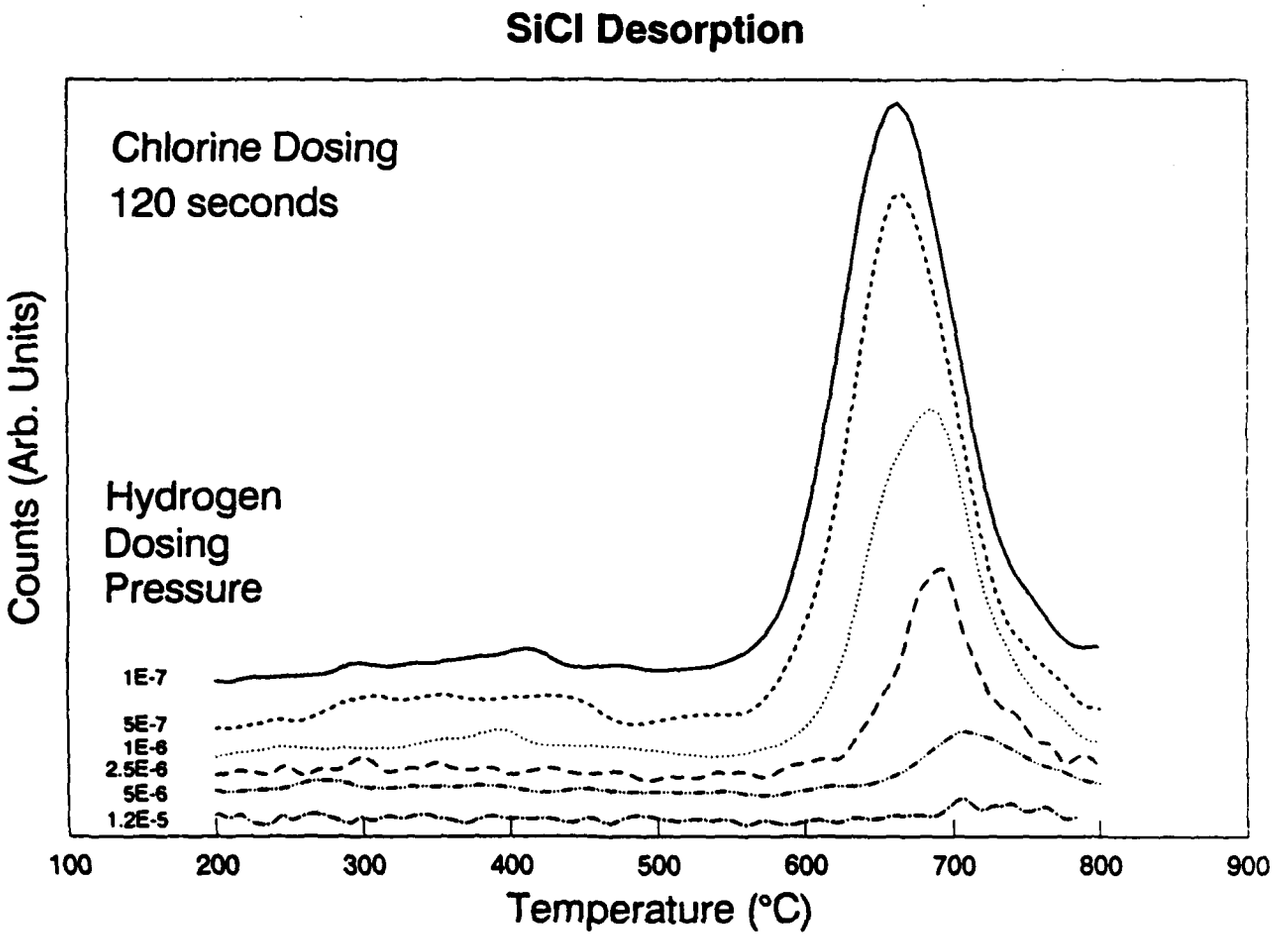

FIGURE 5.2. **These are thermal desorption spectra from the same samples as in Figure 1 except that mass 63, SiCl has been monitored. The reduction in SiCl counts is evident as the hydrogen dose increases.**

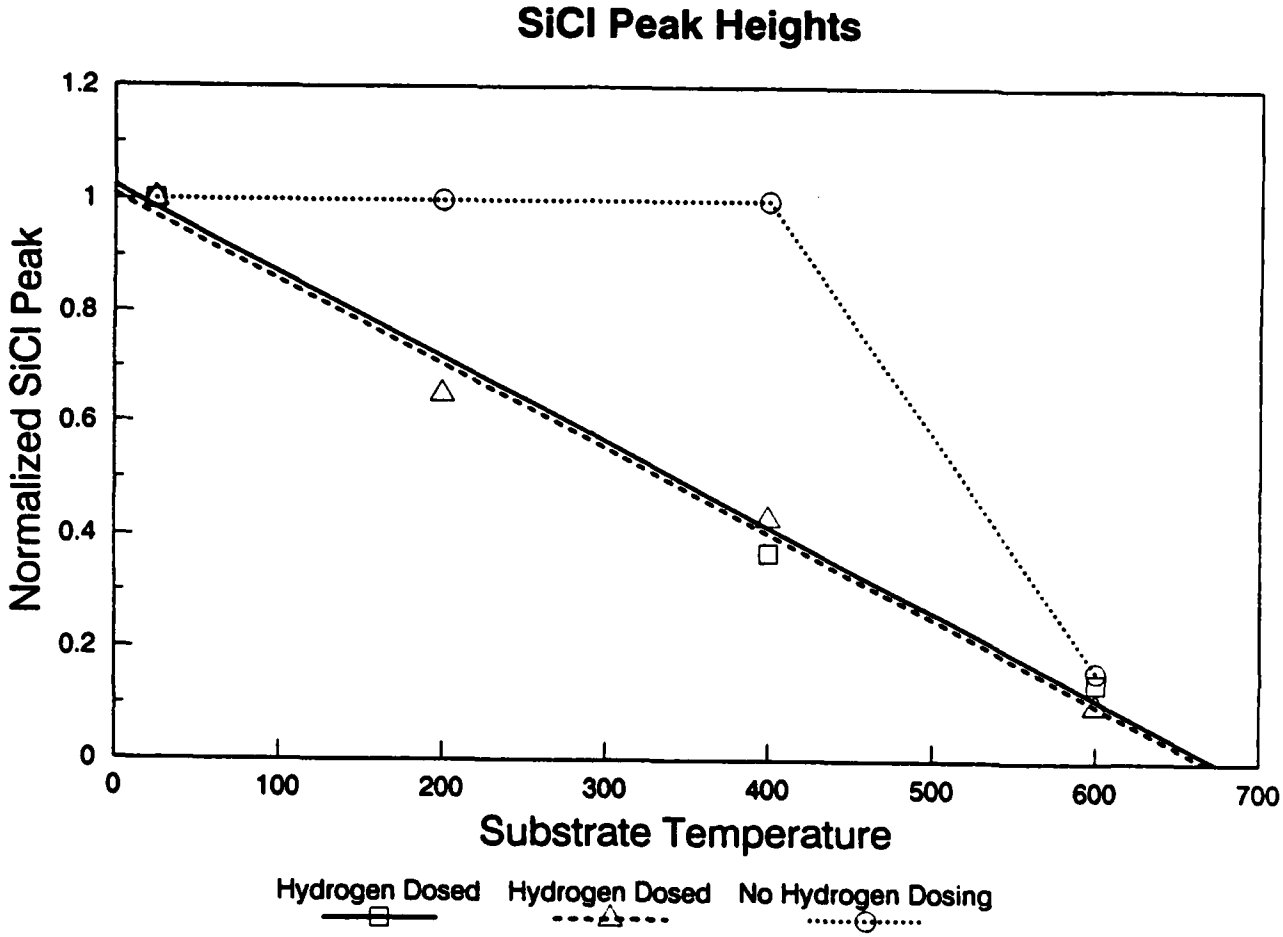

FIGURE 5.3. **This figure displays the relative efficiency of the hydrogen/chlorine extraction process as a function of substrate temperature. The graph compares samples that were dosed with chlorine and then annealed with and without subsequent atomic hydrogen dosing. There is a steady increase in the removal efficiency as the substrate temperature is increased.**

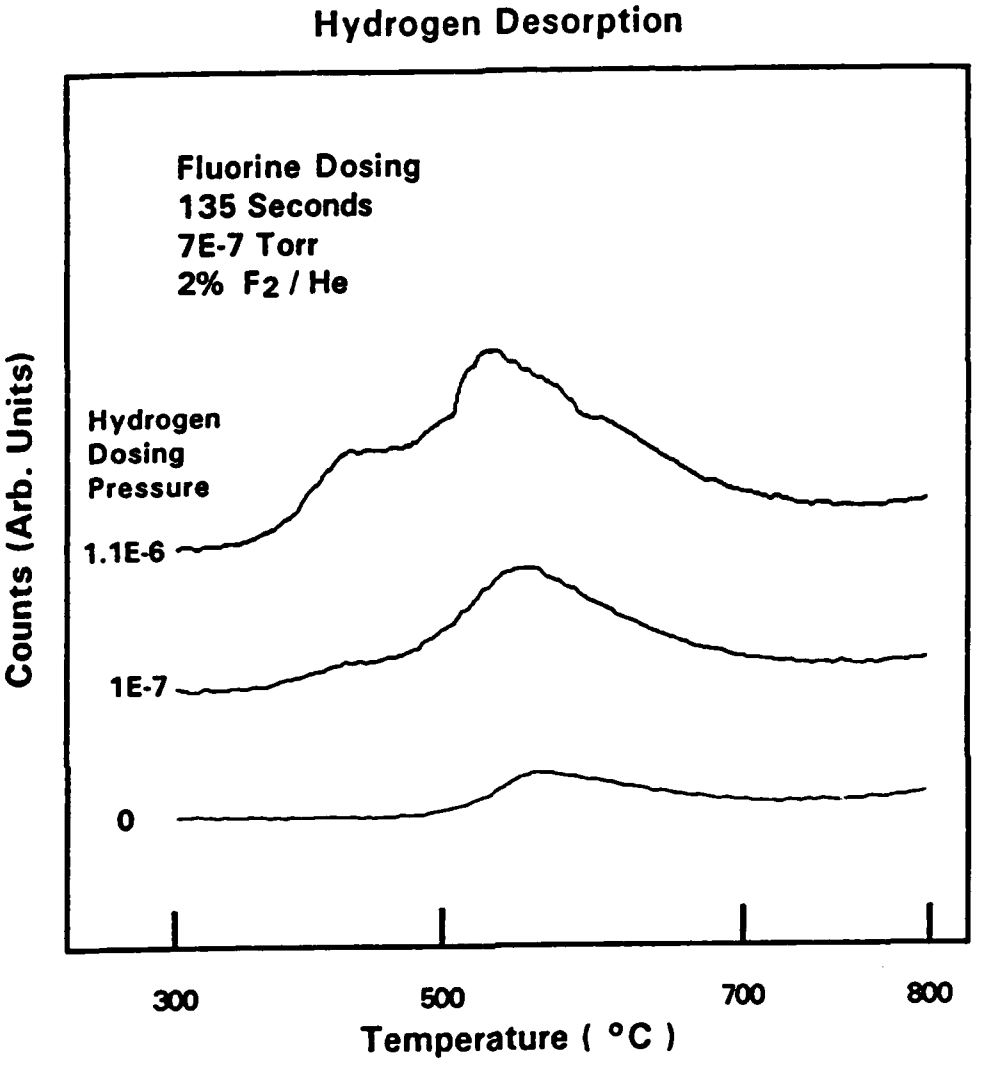

FIGURE 5.4. Hydrogen thermal mass desorption spectra from samples dosed first with molecular fluorine and then atomic hydrogen at the pressures indicated. Two peaks are seen in the desorption spectra corresponding to the two main desorption sites on the silicon (100) surface. There is a small residual hydrogen desorption peak seen in samples that were not dosed with atomic hydrogen. This peak was seen in most samples even after repeated anneals.

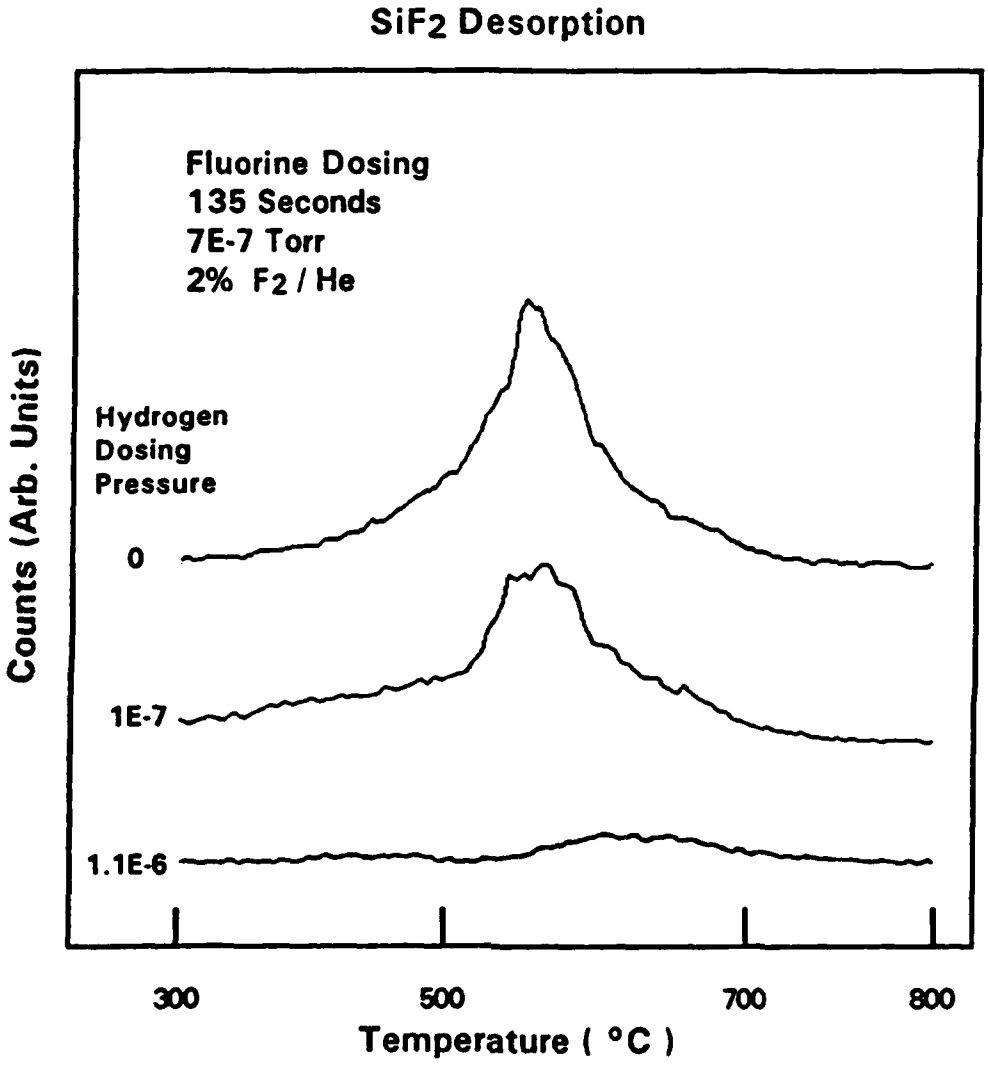

FIGURE 5.5. SiF_2 desorption from same samples as in Figure 5. The samples show a decrease in the SiF_2 desorbed as the total dose of atomic hydrogen increases.

6.0 FABRICATION AND TESTING OF A DIAMOND IGFET

The extremely selective nature of the plasma activated diamond deposition processes provides a very useful and flexible vehicle for device fabrication sequences. Other workers have already reported diamond insulated gate field effect transistor (IGFET) fabrication using selective diamond deposition with a sputtered quartz insulator[1]. In this paper, we report fabrication of a diamond IGFET structure using selective diamond deposition with diborane doping in conjunction with a remote plasma enhanced chemical vapor deposition (RPECVD) of a SiO_2 insulating dielectric layer.

6.1 Device Fabrication

The transistor structure was fabricated on a Type 1A natural diamond (100) substrate from Drucker-Harris. The diamond substrate was cleaned using a conventional RCA wet chemical clean[2]. A 700 A film of polycrystalline silicon was deposited on the substrate. The silicon was patterned using standard lithographic techniques and wet etching to open holes for deposition of the conducting p-type diamond areas. The diamond was deposited using a low pressure rf plasma assisted chemical vapor deposition technique.[1] Following diamond deposition, the silicon mask was etch removed. The sample was then coated with a 250 A RPECVD SiO_2 gate dielectric[3]. Titanium gate electrodes were formed using liftoff. Source drain contact openings were patterned and openings etched in the oxide using buffer HF solution. Titanium contacts were formed using liftoff. The contacts were relatively ohmic as deposited. The gate length and

width of the transistors was 8μm and 50μm, respectively.

The boron doping was characterized by Van derPau Hall measurement of a blanket epitaxial film on a similar Type IA natural diamond (100) substrate. A plot of carrier concentration and mobility vs. temperature is shown in Figure 6.1. Clearly, there are two levels affecting the carrier concentration. The origin of the lower level is not clear at this point in time, but could be due to surface contamination. Diborane doping reported by Fujimori, et al.[4], using a microwave plasma CVD technique, indicates that at an electrically active boron concentration of $1 \times 10^{17}cm^{-3}$, the mobility was severly degraded from that observed for doping concentrations of $10^{14}cm^{-3}$. Using a mobility of 30-60 $cm^2/V-s$, the doping in the FET channel was estimated to be $5 \times 10^{15}cm^{-3}$ to $1 \times 10^{16}cm^{-3}$. The mobilities for the diamond doped with boron are very low, possibly due to compensation or other effects as yet not determined.

The IGFET source-drain IV characteristics are shown in Figure 6.2. The device showed transistor action characteristic of a p channel, depletion mode device. There is some indication of saturation in the 6 to 8 V region. The device cannot be pinched off with the available gate voltage. The leakage current is most likely due to defects in the material or surface leakage. The maximum transconductance of the device is 38 μS/mm at 8 V drain to source. The transconductance of the device is slightly larger for the 1 to 2 V gate step than for the 0 to 1 V gate step. This increase in transconductance with increasing depletion is indicative of a relatively high density of surface states at or near the diamond/SiO_2 interface. The geometry of the FET is such that the source to gate resistance is on the order of 2×10^5 Ω. This resistance would

decrease the transconductance of the device by a factor of about 2.

Characterization of the IGFET device described in this paper indicates that the diamond/SiO_2 interface has a high interface state density leading to degraded device performance. The RPECVD SiO_2 process is currently used to fabricate high performance Si MISFETs ($G_{max} \sim 75$ mS/mm at a gate length of 2 μm with $\mu_{eff} = 800$ cm^2/V-s), thus, more effective surface treatments of the diamond surface either during the termination of the growth or prior to SiO_2 deposition are needed to achieve high performance IGFETs.

1. S.A. Grot, C.W. Hatfield, G. Sh. Gildenblat, A.R. Badzian, and T. Badzian, "Semiconductor Device Development Using Selectively Grown Thin-Film Diamond", presented at the Second International Conference on the New Diamond Science and Technology (ICNDST-2), Washington, DC(USA), September 23-27, 1990.

2. R.A. Rudder, G.C. Hudson, Y.M. LeGrice, M.J. Mantini, J.B. Posthill, R.J. Nemanich, and R.J. Markunas, Mat. Res. Soc. EA-19, 89 (1989).

3. G.G. Fountain, R.A. Rudder, S.V. Hattangady, R.J. Markunas, P.S. Lindorme, J. Appl. Phys. 63, 4744 (1988).

4. N. Fujimori, H. Nakahata, T. Imai, Jap. J. Appl. Phys. 29, 824 (1990).

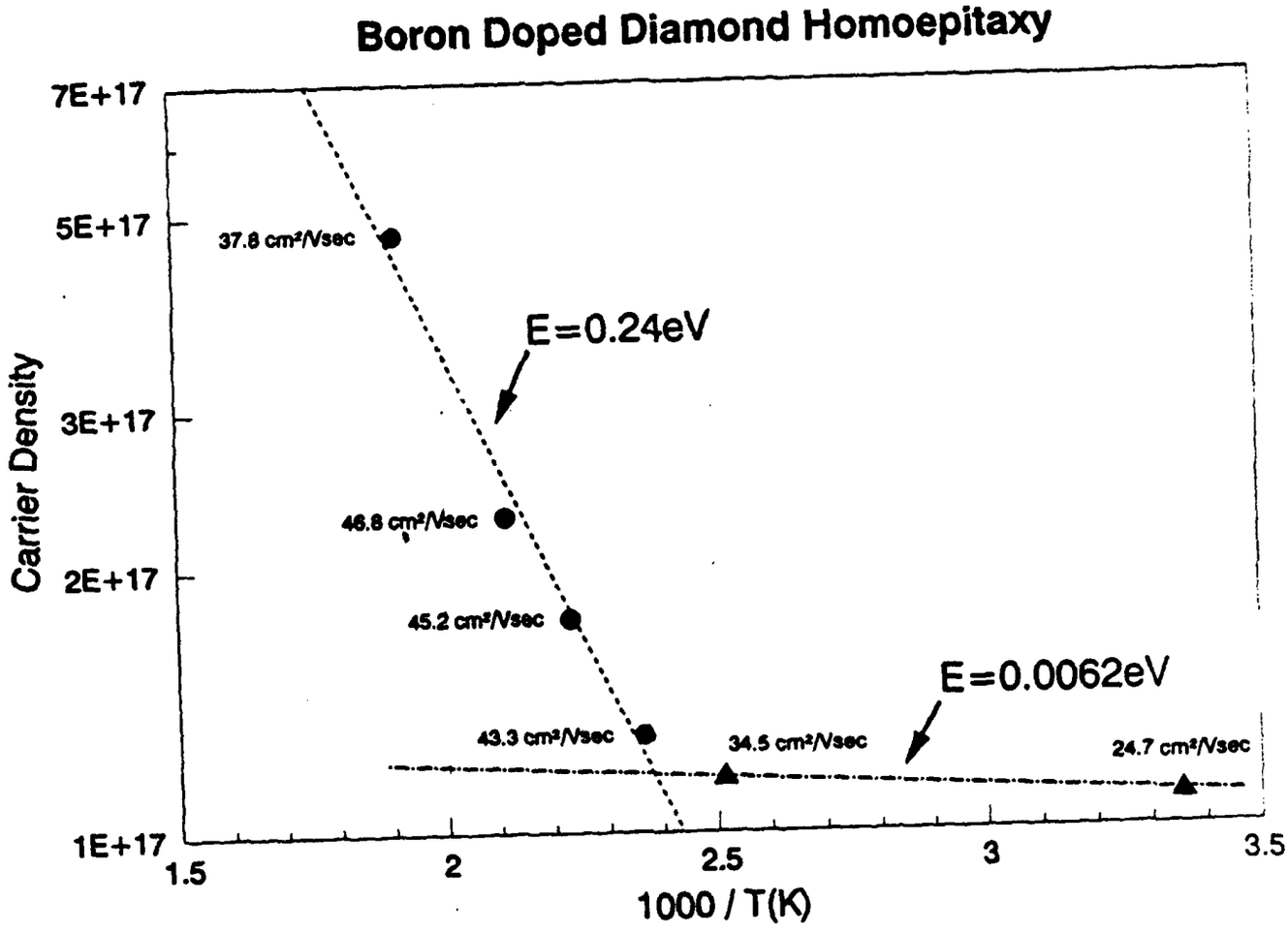

FIGURE 6.1. **Carrier concentration vs. mobility for boron doped homoepitaxial films. B_2H_6 was used as the insitu dopant.**

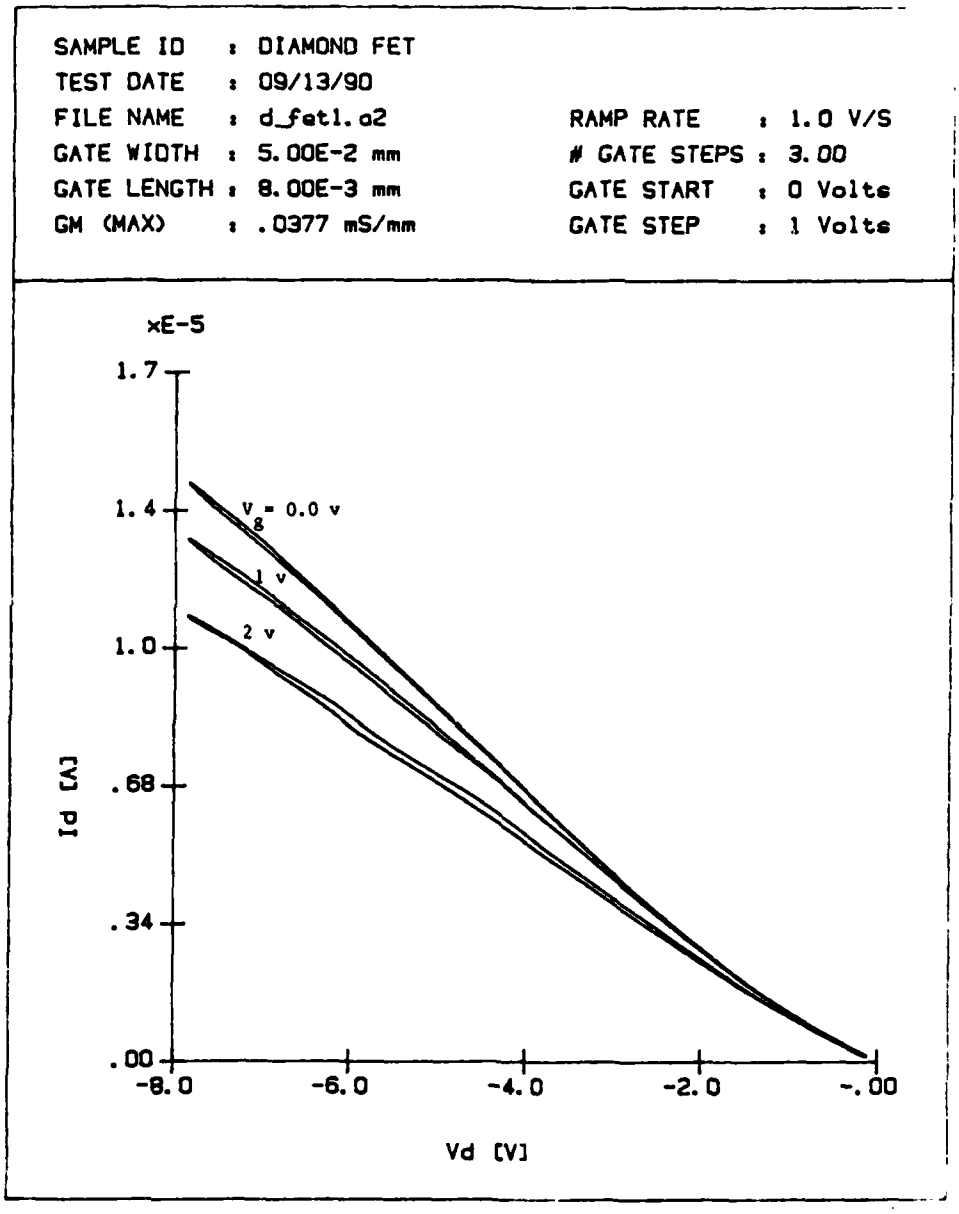

FIGURE 6.2. **Insulated-gate FET source-drain I-V characteristics.**

7.0 INVESTIGATION OF SOLID SOURCE LiF AS AN IN-SITU DOPANT FOR DIAMOND DURING rf PACVD GROWTH

One of the current deficiencies in diamond-based electronics is the lack of suitable n-type dopant. Although there have been specific reports of the formation of n-type diamond[1], this is still an area that requires further development. Li has been proposed as a potential n-type dopant for diamond based on theoretical modelling[2]. We have undertaken a preliminary study to investigate the suitability of using LiF as a solid source to dope diamond growing in a plasma-enhanced chemical vapor deposition (PECVD) environment.

The system used for the growth of homoepitaxial diamond consists of a 13.56 MHz inductively-coupled PECVD system. A gas mixture of 98.5% H_2, 1.0% CO and 0.5% CH_4 flowed through a 62.5 mm quartz tube at a rate of 30 sccm at 5.0 Torr. The sample is positioned near the rf coil on a graphite susceptor and is held at $\sim$ 800 ° C during growth. Type Ia and IIa natural (100) diamond crystals were used in these studies. Lithium doping was accomplished via introduction of a solid source of LiF on the graphite susceptor during the deposition, or via introduction of the solid source to "dose" the reactor prior to loading the substrate for diamond growth. It was found that under diamond growth conditions, the LiF is dissolved by the atomic hydrogen in the reactor. Lithium emissions were observed in the reactor once the sources began to volatilize.

Diamond deposition, with the sources present in the reactor, resulted in high incorporation of Li into the samples ($> 10^{20}$ cm^{-3}). Consequently, growths were

performed with no source of Li in the reactor other than the Li residing on the chamber fixtures following "reactor dosing". Typically, a solid source would be introduced into the reactor, a discharge initiated, whereby emissions of Li could be detected, the solid source removed, and the reactor conditioned with a hydrogen discharge to reduce the Li concentration in the reactor prior to epitaxial growth.

Homoepitaxial films doped with Li were found to be p-type by Hall measurements. For one film, the carrier concentration at room temperature was $\sim 2.8\times10^{16}cm^{-3}$, p-type, with a mobility of $\sim$ 143 cm^2/V-sec. Variable temperature conductivity shows the activation energy, E_a, to be 0.23 eV. We have consistently observed p-type conductivity in diamond homoepitaxial films when Li is introduced in the manner described above. Figure 7.1 shows an I-V trace taken from a Schottky contact (formed by Au evaporation on the surface). This provides further verification of p-type conductivity. There is good rectification, with a breakdown of $\sim$ 6V and a reverse leakage current of $<$ 1 nA. The electron-beam induced current (EBIC) mode of the scanning electron microscope (SEM) was used to estimate the minority-carrier diffusion length. The Schottky contact was used for charge collection, and the induced current was measured as a function of distance, in plan-view, from the contact. Figure 7.2 shows the EBIC trace as function of distance from the Au contact.

For primary beam energies from 10keV - 20 keV, the minority-carrier diffusion length was measured to be 0.5μm. This compares with measured minority-carrier diffusion lengths of $\sim$ 3μm in natural type IIb diamond (B–doped)[3]. Micro-Raman spectroscopy was employed to assess the crystalline quality of homoepitaxial diamond films.

The micro-Raman spectrum shows the 1332 cm^{-1} diamond LO phonon line with a FWHM of 3.0 cm^{-1}. This spectrum was obtained by focusing the incident laser beam (Ar^{+}, 514.5 nm) of $\sim$ 5μm spot size onto the surface of the diamond homoepitaxial film. The 3.0 cm^{-1} Raman line indicates high quality diamond growth. Examining the back side of the diamond substrate also showed a FWHM of 3.0 cm^{-1}.

We currently have no evidence that unintentionally incorporated boron is responsible for the observed p-type conductivity. Films grown without adding a dopant source are so highly resistive that the type cannot be ascertained. Furthermore, the work report herein was done before any intentional introduction of boron into the reactor. We have also observed differences in the mobility and carrier concentration from film to film. Variations in Li concentration due to use of a solid-source for Li doping and/or the variable quality of the diamond substrates are likely reasons for this. It is suggested that future research in this area utilize a liquid or gas phase source for more controlled introduction of Li into the growth environment.

1. Ken Okano, Hideo Kiyota, Tatsuya Iwasaki, Tateki Kurosu, Masamori Iida and Terutaro Nakamura, "Synthesis of N-type Semiconductive Diamond Film and Fabrication of a PN Junction Diode", presented at ICNDST-2, Washington, DC(USA), September 23-27, 1990.

2. J. Bernholc, S. Kajihara, and A. Antonelli, "N-type Doping and Donor Incorporation in Diamond", presented at ICNDST-2, Washington, DC(USA), September 23-27, 1990.

3. D.P. Malta, S.A. Willard, J.B. Posthill, and R.J. Markunas, unpublished results, Research Triangle Institute, 1989.

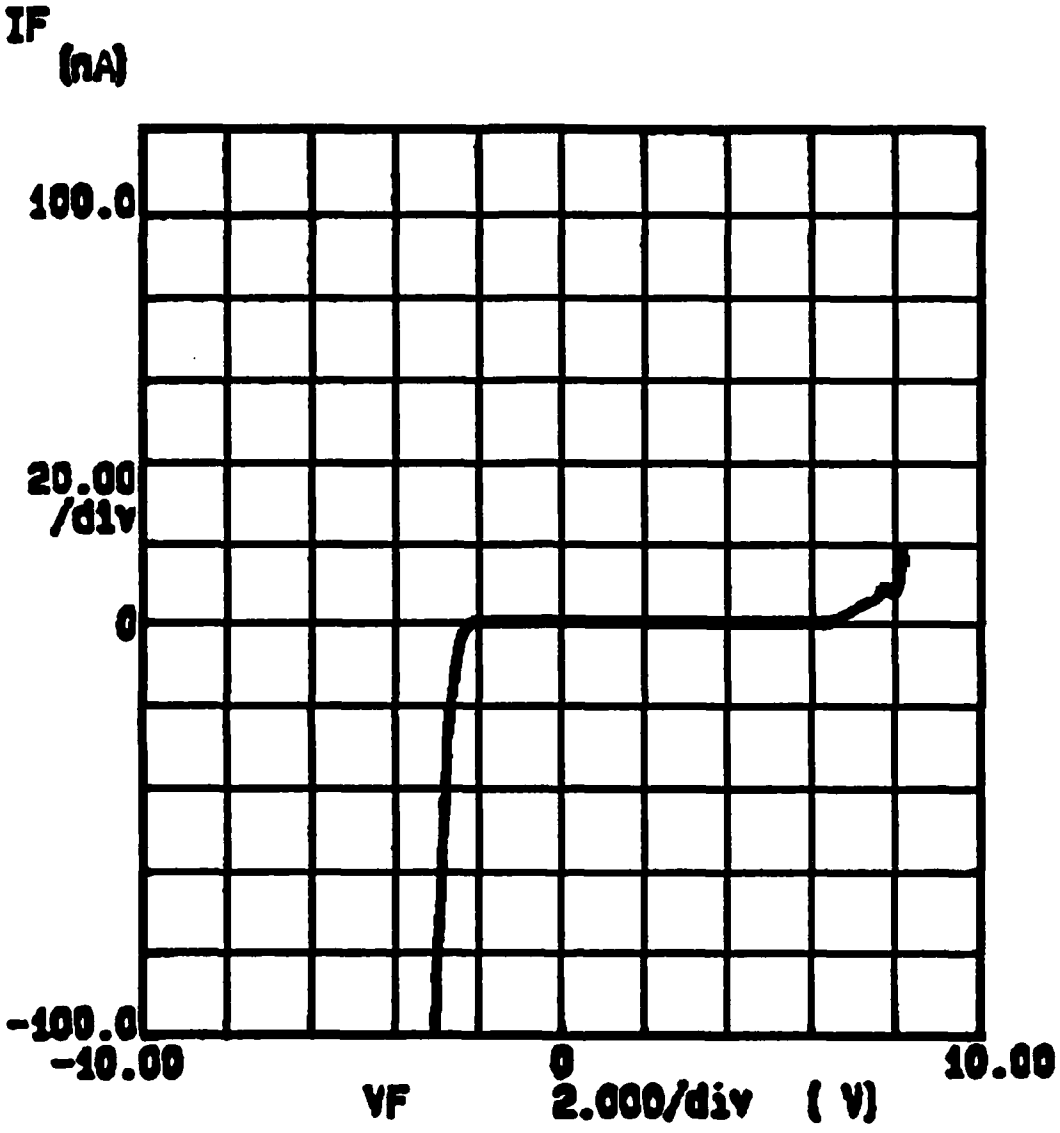

FIGURE 7.1. I-V plot from Li-doped homoepitaxial film grown on (100) diamond. Excellent rectification characteristics are observed.

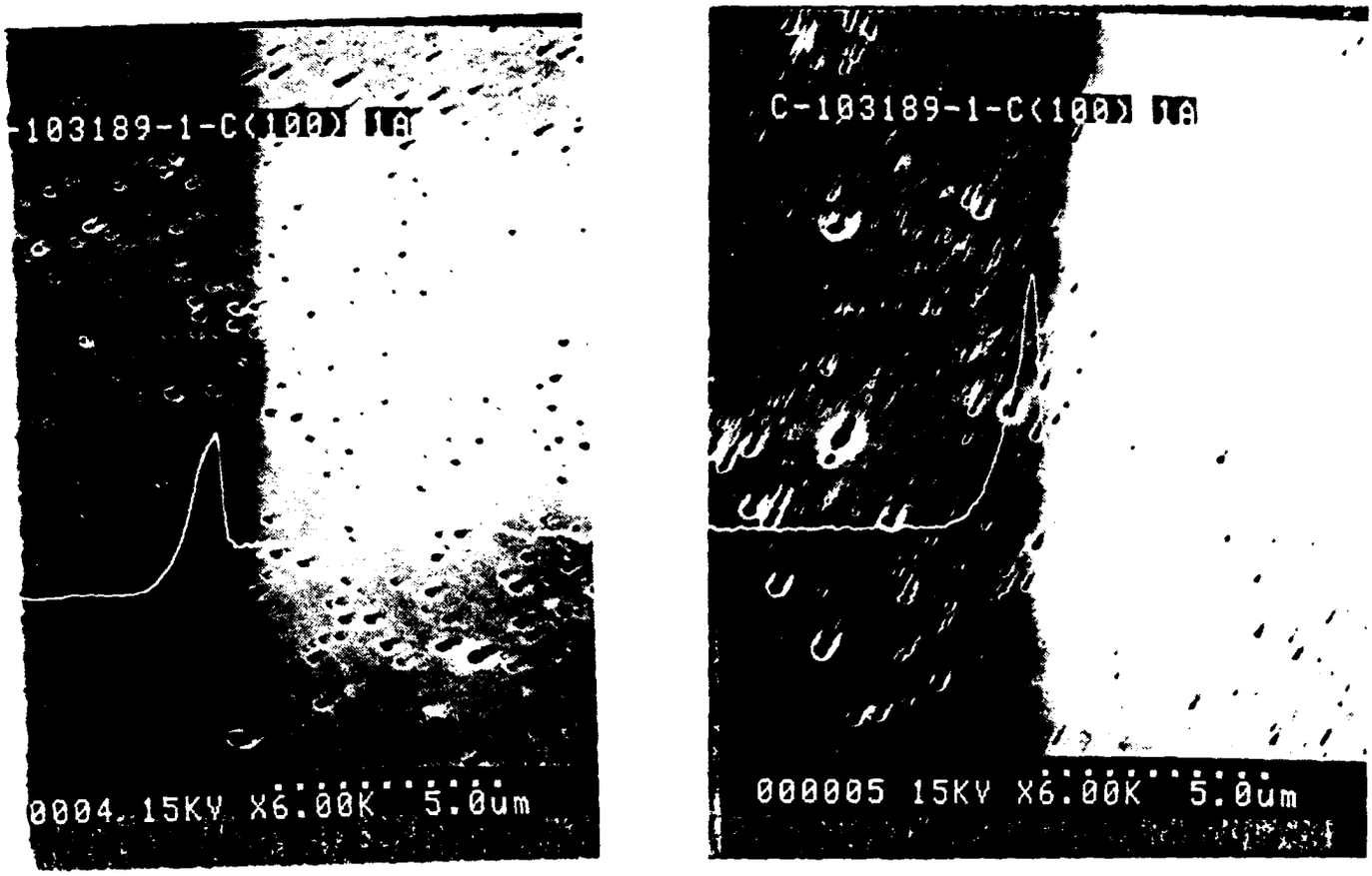

FIGURE 7.2. **Electron beam induced current image near Schottky contact.**